Unit Cube Test for Double Surface Integrals in Frequency Domain Integral Equation Formulations

Mario Cvetković, Dragan Poljak,
Ante Lojić Kapetanović
Faculty of Electrical Engineering, Mechanical
Engineering and Naval Architecture
University of Split, 21000 Split, Croatia
Email: [mcvetkov, dpoljak, alojic00]@fesb.hr

Hrvoje Dodig
Faculty of Maritime Studies
University of Split
21000 Split, Croatia
Email: hdodig@pfst.hr

***Abstract*—The numerical solution of the frequency domain integral equation based formulations require the solution of various double surface integrals. The evaluation of such integrals depends on the distance between the source and observation points, respectively. Many typical integrals can be solved using a numerical integration or a combination of numerical and analytical approach. The paper is on the unit cube test developed for testing various combinations of double surface integrals. Several combinations of source and observation triangles are considered including the far term and near terms, respectively. The numerical solution of integral is facilitated by Gaussian quadrature utilizing the Dunavant's rules for triangles. The extensive tests are carried out to investigate the solution convergence with respect to the increasing frequency and the various utilized discretization schemes.**

***Index Terms*—Integral equation formulation; numerical integration; unit cube test; convergence test; 5G frequencies**

I. Introduction

Accuracy of the numerical solution of integral equation based formulations depends on the precision to which the matrix system elements are calculated. Usually, it is required to solve various double surface integrals, or four dimensional integrals, as they are sometimes called. In addition, it is necessary to take into account how quickly the calculation is carried out. Since numerical efficiency and accuracy are a conflicting demands usually impossible to satisfy at the same time, it is necessary to find a compromise solution between the two.

The advantage of surface integral equation (SIE) formulations such as electric field integral equation (EFIE), magnetic field integral equation (MFIE), or combined field integral equation (CFIE), is in the reduction of problem dimensionality, as well as high accuracy and efficiency. However, its biggest drawback is the singular or nearly singular integrals with kernel containing the Green's function and its derivative. The main reason for the occurrence of numerical instability is due to denominator of Green's function, $R = |\vec{r} - \vec{r}\,'|$, representing the distance between observation point $\vec{r}$ and source point $\vec{r}\,'$, respectively. Depending on the character of integrals that occurs, determining whether the integrand at some point is regular or singular, different strategies are required for their respective solution.

In case of regular integrals, where $\vec{r} \neq \vec{r}\,'$, often the numerical integration is sufficient. For nearly singular integrals, where $\vec{r}$ is very close to $\vec{r}\,'$, oftentimes the solution is to increase the number of integration points or to use a more finer discretization at particular problem location. On the other hand, when $\vec{r} = \vec{r}\,'$, a singular integral occurs, and depending on the singularity type, it is necessary to perform certain mathematical transformations prior to integration itself. For weakly singular integrals, with kernel containing R^{-1}, it is necessary to regularize the kernel before the numerical integration, usually, using methods such as singularity extraction or subtraction [1], [2] or the singularity cancellation technique [3], [4], which includes transformation to polar coordinates or domain transformation. In cancellation methods, this transformation results in Jacobian that cancels the kernel singularity, whereas in the extraction method, the extracted singular part is analytically solved, while residual is solved by numerical means. In case of strongly singular integrals, with kernel containing R^{-2}, a combination of several techniques for weakly singular integrals is required, again followed by numerical integration of the regular part.

When using frequency domain SIE formulations, most often, the complex surface geometry of a problem is described using the triangular patches. This facilitates the use of a so called Rao-Wilton-Glisson (RWG) basis functions particularly developed for triangular patches [5]. Depending on the distance between the triangles defining the positions of the source and the observation points, an appropriate approach to the solution of those integrals is required. In many cases it is not obvious which solution strategy is the most pertinent, as the size and position of interacting triangles will affect the solution accuracy. Moreover, depending on the frequency, it is necessary to represent the problem geometry by using elements of the appropriate size. As the frequency increases, consequently, the size of the element goes down. This in turn results in larger number of elements, resulting in higher computational demands. Hence, the use of a simple straightforward numerical approach when considering regular integrals, or the increase of integration points in case of singular integrals, may not necessarily result in accurate solution at all. Thus, solving these integrals by using simple *brute force* results in

a useless waste of computational resources. Such situations, rather, require a more subtle approach.

This paper is on the set of a suitability tests based on the unit cube devised for testing various integrals arising in the frequency domain integral formulations. The paper is organized as follows: following introductory part, a brief derivation of EFIE for the penetrable object is given as well as the resulting integral equations set. The treatment of various integrals is sketched in the next part, followed by description of the unit cube used for testing several combinations of triangles. Finally, the results of a several convergence tests and the concluding remarks are given.

II. Mathematical Background

A. EFIE Formulation and RWG Basis Function

This paper considers the frequency domain formulation of the electric field integral equation (EFIE), derived from the surface equivalence theorem and the boundary conditions for the electric field:

$$\left[-\vec{E}_n^{sca}(\vec{J},\vec{M})\right]_{tan} = \begin{cases} \left[\vec{E}^{inc}\right]_{tan}, & i=1 \\ 0, & i=2 \end{cases} \tag{1}$$

where E^{inc} is the known electric field incident on the surface of scatterer while the scattered field is denoted by E^{sca} Exterior and interior regions of the problem are denoted with $i = 1, 2$.

More details on the electromagnetic dosimetry model for the lossy homogeneous biological body based on EFIE formulation and RWG basis function can be found in [6]. The following outlines only the important steps related to the present study.

The numerical solution of the EFIE is carried out by an efficient Method of Moments (MoM) scheme reported elsewhere [7]. The tangential component of the scattered electric field is expressed in terms of the equivalent electric and magnetic current densities, $\vec{J}$ and $\vec{M}$, respectively, which are expanded in terms of a linear combination of RWG, and a point wise orthogonal $\hat{n}\times$RWG basis functions, respectively:

$$\vec{J}(\vec{r}) = \sum_{n=1}^{N} J_n \vec{f}_n(\vec{r}); \quad \vec{M}(\vec{r}) = \sum_{n=1}^{N} M_n \vec{g}_n(\vec{r}) \tag{2}$$

where J_n and M_n represent the unknown coefficients, while N is the total number of elements used to discretize the problem surface S.

RWG basis function $\vec{f}_n$, is defined on T_n^+ and T_n^- pair of triangles sharing a common edge, as shown on Fig. 1, and is given by

$$\vec{f}_n^{\pm}(\vec{r}) = \begin{cases} \dfrac{l_n}{2A_n^{\pm}}\vec{\rho}_n^{\pm} & ,\vec{r}\in T_n^{\pm} \\ 0 & ,\vec{r}\notin T_n^{\pm} \end{cases} \tag{3}$$

where l_n is the edge length at the interface between triangles T_n^+ and T_n^-, while A_n^+ and A_n^- denote the surface areas of triangles. Vector $\vec{\rho}_n^+ = \vec{r} - \vec{r}_n^+$ is directed from free vertex of T_n^+ while $\vec{\rho}_n^- = \vec{r}_n^- - \vec{r}$ is directed towards free vertex of T_n^-, as shown on Fig. 1.

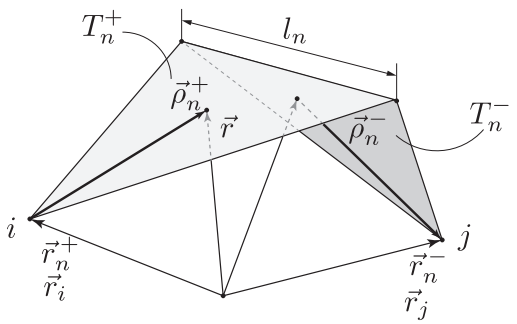

Fig. 1: RWG basis function $\vec{f}_n(\vec{r})$ defined on a pair of triangles in $\mathbf{R}^3$ [5].

Multiplying (1) by testing functions $\vec{f}_m$, where $\vec{f}_m = \vec{f}_n$, and integrating over the surface S, followed by some additional mathematical manipulations [7], [8], yields the following system of a linear equations

$$\sum_{n=1}^{N}\left(j\omega\mu_i A_{mn,i} + \frac{j}{\omega\varepsilon_i}B_{mn,i}\right)J_n + \\ + \sum_{n=1}^{N}\left(C_{mn,i} + D_{mn,i}\right)M_n = \begin{cases} V_m & ,i=1 \\ 0 & ,i=2 \end{cases} \tag{4}$$

which can be written in matrix form as

$$[\mathbf{Z}]\cdot\{\mathbf{I}\} = \{\mathbf{V}\} \tag{5}$$

where $\mathbf{Z}$ is the $2N\times 2N$ system matrix, while $\mathbf{V}$ is the source vector of a dimension $2N$.

B. Double Surface Integrals

When determining elements of system matrix $\mathbf{Z}$, it is necessary to solve the integrals of the following form:

$$A_{mn} = \iint_S \vec{f}_m(\vec{r})\cdot\iint_{S'}\vec{f}_n(\vec{r}\,')G(\vec{r},\vec{r}\,')\,dS'\,dS \tag{6}$$

$$B_{mn} = \iint_S \nabla_S\cdot\vec{f}_m(\vec{r})\iint_{S'}\nabla'_S\cdot\vec{f}_n(\vec{r}\,')G(\vec{r},\vec{r}\,')\,dS'\,dS \tag{7}$$

$$C_{mn} = \pm\frac{1}{2}\iint_S \vec{f}_m(\vec{r})\cdot\left[\hat{n}\times\vec{g}_n(\vec{r})\right]\,dS \tag{8}$$

$$D_{mn} = \iint_S \vec{f}_m(\vec{r})\cdot\iint_{S'}\vec{g}_n(\vec{r}\,')\times\nabla' G(\vec{r},\vec{r}\,')\,dS'\,dS \tag{9}$$

where $\vec{f}_m$ is test function, while $\vec{f}_n$ and $\vec{g}_n$ are basis functions expanded over triangles T_m and T_n, respectively. Observation and source points are denoted by $\vec{r}$ and $\vec{r}\,'$, respectively.

$G(\vec{r},\vec{r}\,')$ represents Green's function for the homogeneous medium

$$G(\vec{r},\vec{r}\,') = \frac{e^{-jkR}}{4\pi R}; \quad R = |\vec{r} - \vec{r}\,'| \tag{10}$$

where R is the distance from observation to source point, while k is the wave number.

Depending on the distance between triangles T_m and T_n, an appropriate approach to the solution of integrals (6)–(9) is required, as depicted on Fig. 2.

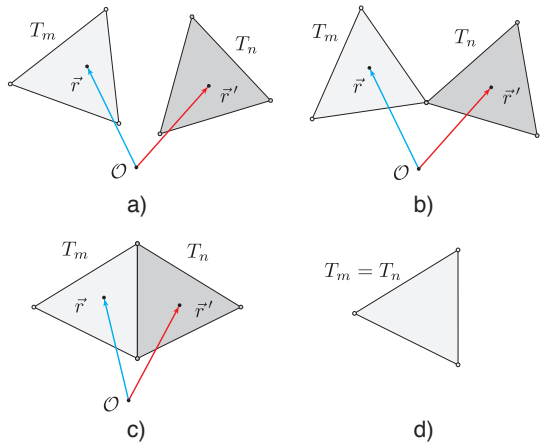

Fig. 2: Integration on several possible combinations of source and observation triangles. a) No common points - far terms, b) Sharing a vertex - near terms, c) Sharing an edge - near terms, d) Overlapping triangles - self terms.

Several combinations are evident from Fig. 2, for which the following solution techniques are used: a) Far terms - if observation and source triangles are far enough, numerical integration is used; b) and c) Near terms - when triangles are close to each other and sharing vertex or edge, combination of analytical and numerical integration is used; d) Self terms - case with overlapping triangles can be solved either analytically, numerically or using combination of the two.

C. Unit Cube Test

The triangle combinations introduced on Fig. 2 can be depicted using any of the canonical geometries, such as e.g. sphere, cylinder or ellipsoid, which can be latter utilized as a simple geometrical representations of human head, trunk or complete body. Instead, as an initial effort, a cubical shape is used in this work, as it enables a very simple control of the meshing procedure. Each side of the unit length cube can be meshed using 8 isosceles triangles, i.e. total of 48 triangles for the complete cube, as shown on Fig. 3.

Various combinations of triangle pairs, including coplanar and orthogonal, far, near, and self terms, respectively, can be selected. The following combination of triangles can be seen on Fig. 3: coplanar far pair (triangles 1 and 2, i.e. 1-2), coplanar near pairs (3-4 and 1-3), self pair (1-1), orthogonal far pair (1-5), orthogonal near pairs (1-6 and 1-7). All said combinations are also listed in Table I as well as a proposed integration order according to [9].

Furthermore, the introduced unit cube and the associated triangles can be easily scaled down to facilitate testing of

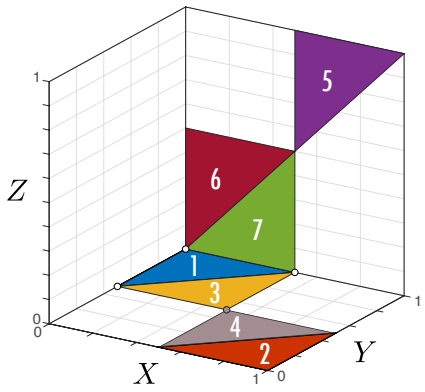

Fig. 3: Unit cube for testing various triangle combinations: coplanar and orthogonal combinations obtained by selecting triangle pairs from two sides of cube.

numerical integration rules for various integrals at different frequency of interest. Figure 4 illustrates the comparison of triangular element size when unit cube scale is halved in several iteration steps ($n = 1, \ldots, 8$). It should be noted that discretisation steps numbered $n = 4, 5, 6, 7, 8$ correspond to discretisation scheme latter denoted as: $1/8$, $1/16$, $1/32$, $1/64$, and $1/128$, respectively.

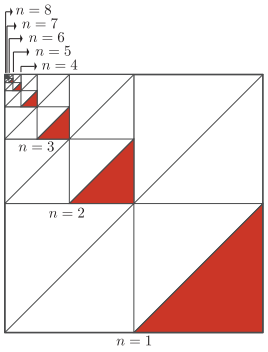

Fig. 4: Illustration of triangular element size on one side of unit qube, depending on the scaling iteration number $n = 1, \ldots, 8$.

D. Numerical Integration

As already mentioned, depending on the distance between the source and the observation triangles, the solution of integrals (6)–(9) can be carried out purely numerically in case of far triangles pair, or by a combination of analytical and numerical approach.

In case of numerical integration, (6)–(9) can be solved by means of Gaussian quadrature on triangles, using the following expressions:

$$A_{mn} = \frac{l_m l_n}{16\pi} \sum_{p=1}^{M} \sum_{q=1}^{N} w_p w_q \vec{\rho}_m^{\pm}(\vec{r}_p) \cdot \vec{\rho}_n^{\pm}(\vec{r}\,'_q) \frac{e^{-jkR_{pq}}}{R_{pq}} \tag{11}$$

$$B_{mn} = (\pm)\frac{l_m l_n}{4\pi} \sum_{p=1}^{M} \sum_{q=1}^{N} w_p w_q \frac{e^{-jkR_{pq}}}{R_{pq}} \tag{12}$$

	Triangle combination						
Integral and approach	**FAR** (0), $\|\|$	**NEAR** (1), $\|\|$	**NEAR** (1), $\|\|$	**SELF** (3), $\|\|$	**FAR** (0), $\perp$	**NEAR** (1), $\perp$	**NEAR** (2), $\perp$
Amn numerical	5,4	5,4	Real	-	5,4	5,4	Real(10,4?)
Amn singext num/anl	4	4	12	12	4	6	4
Amn singext numerical	5,4	5,4	Real	-	5,4	5,4	Real(10,4?)
Bmn numerical	5,4	5,4	Real	-	5,4	5,4	Real(10,10?)
Bmn singext num/anl	4	4	12	6	4	4	4
Bmn singext numerical	5,4	5,4	Real	-	5,4	5,4	5,4
Cmn numerical	2	2	2	2	=0	=0	=0
Dmn numerical	=0	=0	=0	=0	5,4	5,6	Re(10,14?)
Dmn numerical 1	=0	=0	=0	=0	4,4	4,4	4,4
Dmn numerical 2	=0	=0	=0	=0	4,4	4,4	4,4

TABLE I: One possible approach (*strategy*) applied for the solution of various integrals and triangle combinations used in high frequency electromagnetic-thermal dosimetry [9]. **FAR** = Far triangles, **NEAR** = Near triangles, sharing either vertex or edge, **SELF** = Overlapping triangles, (N) = number of shared points, $||$ - coplanar, $\perp$ - orthogonal, $= 0$ - equal to zero, **Real** - unstable part of solution, **singext** - singularity extraction, **num/anl** - combination of numerical and analytical approach.

$$C_{mn} = \mp \frac{l_m l_n}{8A_n^{\pm}} \sum_{p=1}^{M} w_p \vec{\rho}_m^{\pm}(\vec{r}_p) \cdot \vec{\rho}_n^{\pm}(\vec{r}_p) \tag{13}$$

$$D_{mn} = \frac{l_m l_n}{16\pi} \sum_{p=1}^{M} \sum_{q=1}^{N} w_p w_q \vec{\rho}_m^{\pm}(\vec{r}_p) \cdot \left[\hat{n}' \times \vec{\rho}_n^{\pm}(\vec{r}_q')\right] \times \times \left(\vec{r}_p - \vec{r}_q'\right) (1 + jkR_{pq}) \frac{e^{-jkR_{pq}}}{R_{pq}^3} \tag{14}$$

with $R_{pq} = |\vec{r}_p - \vec{r}_q'|$, where $\vec{r}_p$, $\vec{r}_q'$, w_p and w_q denote the location of Gaussian points and weights for the source and observation triangles, respectively. M and N, represent the number of integration points for the source and observation triangle, respectively, dependent on the order of integration, $P = 1, \ldots, 20$, and $Q = 1, \ldots, 20$.

The quadrature points and the associated weights are chosen according to Dunavant's symmetric quadrature rules for triangles and rules of degree up to $P = 20$ can be found in [10].

On the other hand, when source and observation triangles are close, such as when sharing a common vertex or an edge, the integrands of (6)–(9) become singular, when $\vec{r} \to \vec{r'}$. In that case, one of the approach is to regularise the Green's function by rewriting

$$\frac{e^{-jkR}}{R} = \frac{e^{-jkR} - 1}{R} + \frac{1}{R} \tag{15}$$

Inserting (15) e.g. into (6), one obtains:

$$A_{mn} = \frac{l_m l_n}{16 A_m^{\pm} A_n^{\pm}} \left[\iint_S \vec{\rho}_m^{\pm}(\vec{r}) \cdot \iint_{S'} \vec{\rho}_n^{\pm}(\vec{r}') \frac{(e^{-jkR} - 1)}{R} \, dS' \, dS + + \iint_S \vec{\rho}_m^{\pm}(\vec{r}) \cdot \iint_{S'} \vec{\rho}_n^{\pm}(\vec{r}') \frac{1}{R} \, dS' \, dS \right] \tag{16}$$

The first term from (16) can be solved numerically, as $R \to 0$ in the limiting case, while the second term can be solved analytically, using a closed form solution from [11].

Similar approach can be applied to integrals in (7) and (9), as well.

III. Results

Utilizing the unit cube introduced in the preceding section, the following results are obtained. The first set of results, shown on Fig. 5 are related to numerical solution of double surface integral (6) in case of far triangles and near triangles sharing an edge, numbered (1-2) and (1-3), respectively, as depicted on Fig. 3. The numerical solutions are obtained using various integration orders P and Q for source and observation triangles, respectively, with $P = 1, \ldots, 20$ and $Q = 1, \ldots, 20$.

The unit cube is first scaled such that $a = \lambda/5$, $b = a/2$, where a is the length of cube side, and b is the length of triangle edge, while λ is the wavelength. Regardless of frequency (300 MHz - 90 GHz), in case of a constant electrical length, i.e. $ka = const.$, both real and imaginary part of the solution converges identically. As clearly seen on Fig. 5a), obtained at 6 GHz, increasing the number of integration points, results in the convergence on the real and imaginary part of the solution. This can be also seen on Fig. 5b) where the solution is represented by the grey colour shade on a (P, Q) square, where the increase of integration order is from left to right for Q, and from top to bottom for P. It should be noted here, when considering the (P, Q) square, the gray colour itself is not essential. Rather, the colour of the complete square is. If, going from top left to bottom right, the shade of grey becomes uniform, the solution converges. On the other hand, checkered pattern means that the convergence can not be guaranteed and particular care should be taken.

Compared to situation with far triangle pairs, when using a purely numerical approach to solve the near triangle pairs, as evidenced from Fig. 5c), the real part of the solution behaves rather erratic at low integration orders. Only when integration orders on both triangles are increased to 10-12, does the solution start to converge. The very slow convergence of the solution is evidenced by the checkered pattern, as shown on Fig. 5d).

The following results are obtained without the scaling of unit cube geometry. Two frequencies are considered, 0.7 GHz and 3.6 GHz, related to frequency spectrum of 5th generation of mobile communications, as utilized in Croatia. To keep presentation brief, only convergence results given by (P, Q) squares are presented. Three combinations of triangle pairs are considered, and the results are shown on Fig. 6.

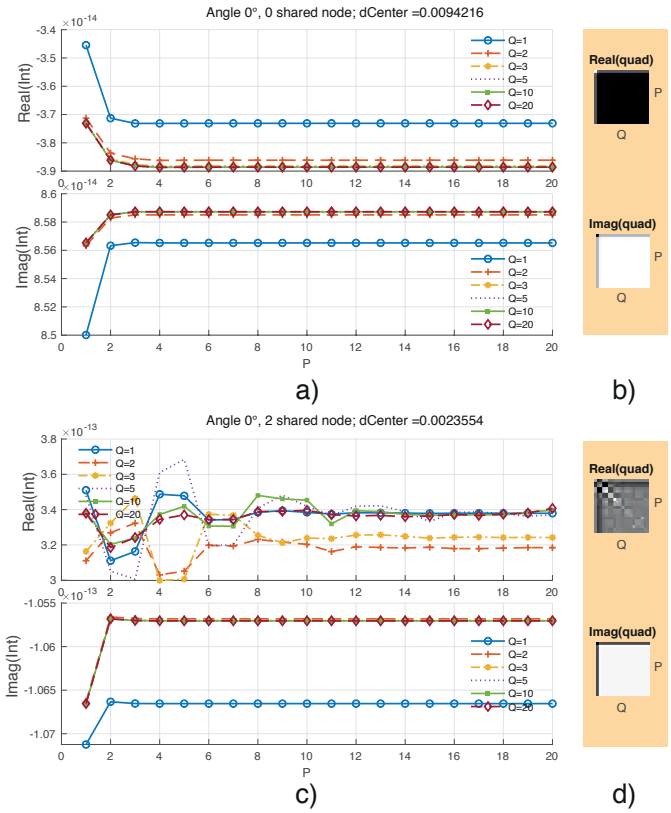

Fig. 5: Convergence of real and imaginary part of integral using several quadrature orders ($Q = 1, 2, 3, 5, 10, 20$), a) Far triangles, c) Near triangles sharing an edge. Visualization of b) Far and d) Near triangles' interaction using a PQ–square.

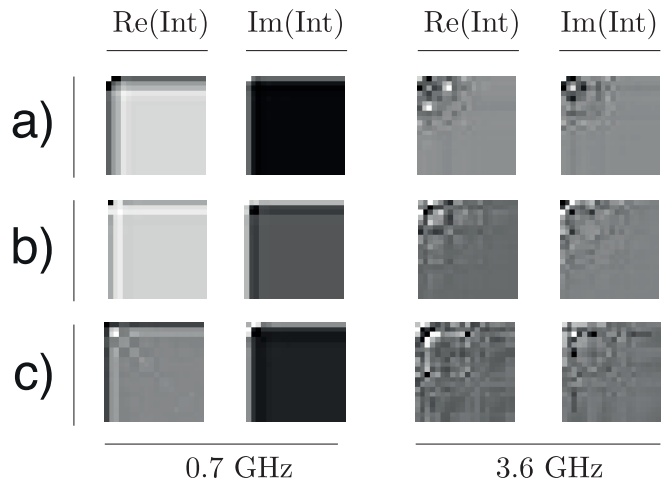

Fig. 6: Effect of triangle distance. Convergence of integral A_{mn} at two selected frequencies: 0.7 and 3.6 GHz. Combination of coplanar triangles (triangle numbers): a) sharing no points (1 and 2), b) sharing a vertex (3 and 4), c) sharing an edge (1 and 3).

As seen from the results obtained at 0.7 GHz, in case of a near triangles sharing an edge, as depicted on Fig. 6c), higher integration order is necessary to ensure the convergence of the results. However, as shown on Fig. 6b)-c), if the triangle size is not sufficiently small, compared to wavelength of interest (3.6 GHz in this case), in case of near triangles, even higher integration rules do not warrant the convergence. Thus, more finer discretization of the problem geometry should be utilized.

The final set of results is related to the effect of surface discretization. Integral (6) is again solved using Gaussian quadrature with varying integration order, using several discretization schemes of unit cube: $1/8$, $1/16$, $1/32$, $1/64$, and $1/128$. The results are shown on Fig. 8.

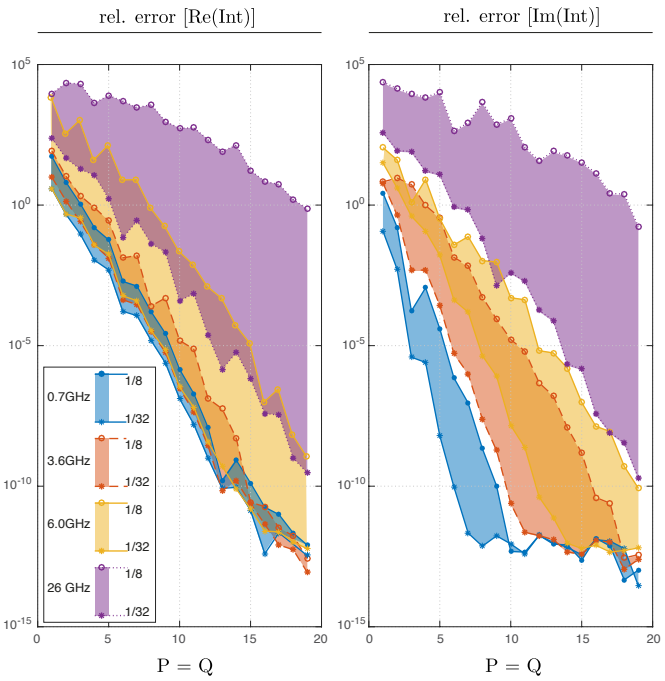

Fig. 7: Comparison of the solution convergence at several 5G frequencies using $1/8$ and $1/32$ discretization schemes. Relative error of the solution real and imaginary part wrt. $P = 20, Q = 20$ integration rule.

The results are obtained at the following frequencies: 0.7 GHz, 3.6 GHz, 6 GHz, 26 GHz, and 90 GHz. As seen from Fig. 8, if coarser mesh is utilized ($1/8$ and $1/16$), the convergence of the solution at higher frequencies (26 GHz and 90 GHz) questionable, at best. On the other hand, using more finer mesh ($1/32$, $1/64$, $1/128$), even at very high frequencies such as 90 GHz, lower integration orders can be used. However, simply utilizing a more finer mesh, results in the significantly increased computational requirements, due to a fully populated system matrices arising from the use of integral equation formulations.

Finally, the decision on which level of discretization to use will depend not only on the required level of accuracy but also on the computational resources available. As seen on Fig. 7, where relative error of particular (P, Q) integration order combination are given with respect to $P = 20, Q = 20$

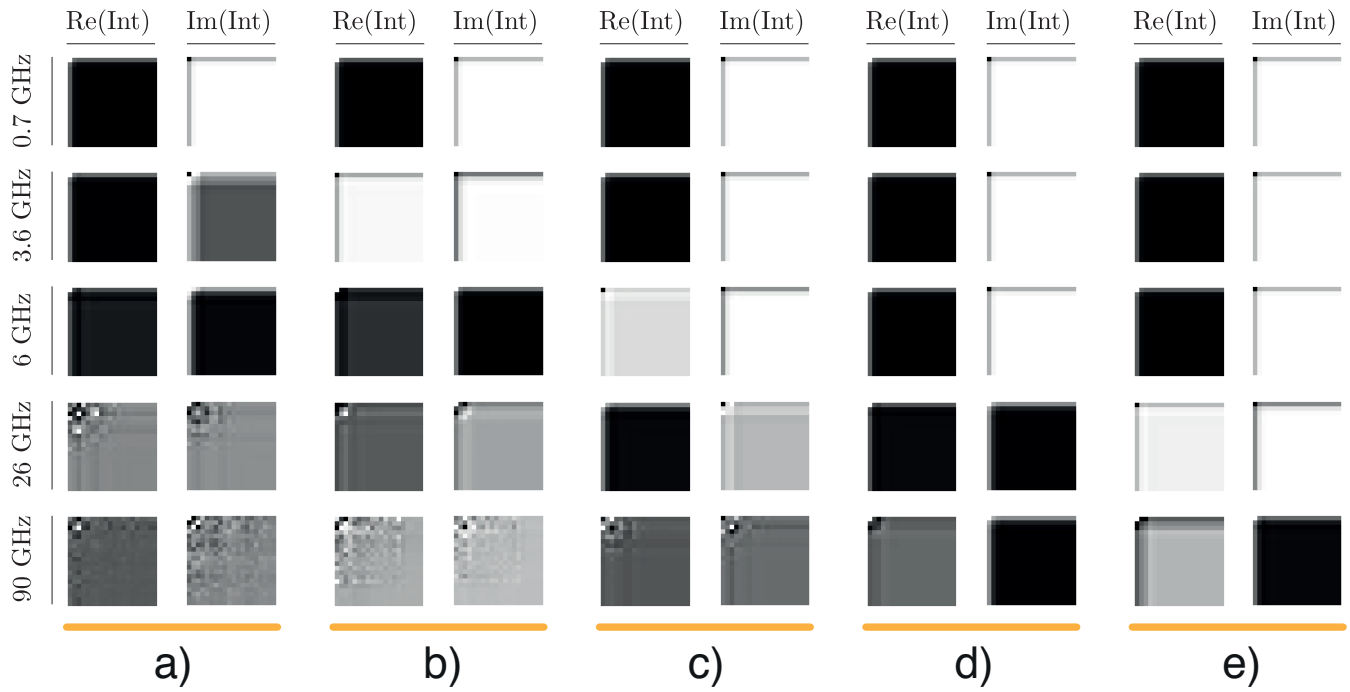

Fig. 8: Effect of surface discretization. Convergence of integral A_{mn} with respect to frequency, using several discretization schemes: a) $1/8$, b) $1/16$, c) $1/32$, d) $1/64$, e) $1/128$. Each square (real and imaginary part at particular frequency includes integration orders from $P = 1 \ldots 20, Q = 1 \ldots 20$.

integration rule, at frequencies below 6 GHz, the decision is still open between finer discretization versus higher integration rule. However, the higher the frequency, the slower the solution converges. At 26 GHz, if the required relative error is e.g. below $\epsilon = 10^{-5}$, the only option is to use finer mesh, as even the highest quadrature rules converge very slowly.

IV. Conclusion

This paper presented the unit cube test pertinent for testing various double surface integrals arising from the frequency domain integral equation formulations. Several combinations of source and observation triangles are considered including the far term and near terms, respectively. The numerical solution of double surface integral is carried out using the double Gaussian quadrature employing the Dunavant's rules for triangles. The results of the extensive tests suggest that, based on the use of pure numerical integration, the solution converges more slowly with the increasing frequency, and the only way to increase the rate of convergence is to use finer discretization, i.e. smaller elements. The future work should thus consider the best approach from the computational resources point of view.

References

[1] M. Khayat and D. Wilton, "Numerical evaluation of singular and near-singular potential integrals," *IEEE Transactions on Antennas and Propagation*, vol. 53, no. 10, pp. 3180–3190, 2005.

[2] S. Jarvenpaa, M. Taskinen, and P. Yla-Oijala, "Singularity subtraction technique for high-order polynomial vector basis functions on planar triangles," *IEEE Transactions on Antennas and Propagation*, vol. 54, no. 1, pp. 42–49, Jan 2006.

[3] R. Graglia, "On the numerical integration of the linear shape functions times the 3-D Green's function or its gradient on a plane triangle," *IEEE Transactions on Antennas and Propagation*, vol. 41, no. 10, pp. 1448–1455, 1993.

[4] L. Li and T. F. Eibert, "Radial-angular singularity cancellation transformations derived by variable separation," *IEEE Transactions on Antennas and Propagation*, vol. 64, no. 1, pp. 189–200, Jan 2016.

[5] S. Rao, D. R. Wilton, and A. Glisson, "Electromagnetic scattering by surfaces of arbitrary shape," *IEEE Transactions on Antennas and Propagation*, vol. 30, no. 3, pp. 409–418, May 1982.

[6] M. Cvetković and D. Poljak, "Electromagnetic dosimetry based on EFIE formulation and RWG basis function," *Boundary Elements and other Mesh Reduction Methods XLI*, vol. 122, p. 143, 2019.

[7] M. Cvetković and D. Poljak, "An efficient integral equation based dosimetry model of the human brain," in *Proceedings of 2014 International Symposium on Electromagnetic Compatibility (EMC EUROPE) 2014, Gothenburg, Sweden, 1-4 September 2014*, 2014, pp. 375–380.

[8] M. Cvetković, D. Poljak, and J. Haueisen, "Analysis of transcranial magnetic stimulation based on the surface integral equation formulation," *Biomedical Engineering, IEEE Transactions on*, vol. 62, no. 6, pp. 1535–1545, June 2015.

[9] M. Cvetković, "Method for electromagnetic thermal dosimetry of the human brain exposed to high frequency fields (in croatian)," Ph.D. dissertation, University of Split, Croatia, 2013.

[10] D. A. Dunavant, "High degree efficient symmetrical gaussian quadrature rules for the triangle," *International Journal for Numerical Methods in Engineering*, vol. 21, no. 6, pp. 1129–1148, 1985.

[11] D. R. Wilton, S. Rao, A. W. Glisson, D. Schaubert, O. Al-Bundak, and C. Butler, "Potential integrals for uniform and linear source distributions on polygonal and polyhedral domains," *IEEE Transactions on Antennas and Propagation*, vol. 32, no. 3, pp. 276–281, 1984.